Contribution of Cation−π Interactions to Protein Stability†

Ravindra S. Prajapati,‡ Minhajuddin Sirajuddin,‡ Venuka Durani,‡ Sridhar Sreeramulu,‡ and Raghavan Varadarajan*,‡,§

Molecular Biophysics Unit, Indian Institute of Science, Bangalore 560 012, India, and Chemical Biology Unit, Jawaharlal Nehru Center for Advanced Scientific Research, Jakkur, P.O., Bangalore 560 004, India

Received June 26, 2006; Revised Manuscript Received September 30, 2006

ABSTRACT: Calculations predict that cation−π interactions make an important contribution to protein stability. While there have been some attempts to experimentally measure strengths of cation−π interactions using peptide model systems, much less experimental data are available for globular proteins. We have attempted to determine the magnitude of cation−π interactions of Lys with aromatic amino acids in four different proteins (LIVBP, MBP, RBP, and Trx). In each case, Lys was replaced with Gln and Met. In a separate series of experiments, the aromatic amino acid in each cation−π pair was replaced by Leu. Stabilities of wild-type (WT) and mutant proteins were characterized by both thermal and chemical denaturation. Gln and aromatic → Leu mutants were consistently less stable than corresponding Met mutants, reflecting the nonisosteric nature of these substitutions. The strength of the cation−π interaction was assessed by the value of the change in the free energy of unfolding [$\Delta\Delta G^\circ = \Delta G^\circ$(Met) − ΔG°(WT)]. This ranged from +1.1 to −1.9 kcal/mol (average value −0.4 kcal/mol) at 298 K and +0.7 to −2.6 kcal/mol (average value −1.1 kcal/mol) at the T_m of each WT. It therefore appears that the strength of cation−π interactions increases with temperature. In addition, the experimentally measured values are appreciably smaller in magnitude than calculated values with an average difference $|\Delta G^\circ_{expt} - \Delta G^\circ_{calc}|_{av}$ of 2.9 kcal/mol. At room temperature, the data indicate that cation−π interactions are at best weakly stabilizing and in some cases are clearly destabilizing. However, at elevated temperatures, close to typical T_m's, cation−π interactions are generally stabilizing.

Current predictive ability of protein structure from amino acid sequence is limited in part due to the lack of quantitative understanding of the different factors which define a single low-energy fold. A typical globular protein is stable by only 5−10 kcal/mol with respect to its unfolded state (*1*). A folded protein is stabilized by a number of noncovalent interactions such as hydrophobic interactions, hydrogen bonds, salt bridges, and cation−aromatic (cation−π) interactions. The relevance of cation−π interactions in biological systems has been recognized in recent years. Positively charged amino groups of Lys, Arg, or His are often preferentially located within 6 Å of the ring centroids of Phe, Tyr, or Trp (*2*). Further experimental support for the importance of cation−π interactions came from observations that the neurotransmitter acetylcholine could bind with a completely hydrophobic synthetic receptor comprising of primarily aromatic amino acid residues (*3*) and from other studies where unnatural amino acids were used for studying cation−π interactions (*4*−*6*). Cation−π interactions have recently been observed in many biological systems including proteins (*7*), protein−DNA complexes (*8*), and ion channels (*4*, *9*) as well as in enzyme catalysis and molecular recognition (*10*). Cation−π interactions have also been implicated as a stabilizing factor in proteins from hyperthermophiles based on genome sequence analysis (*11*). Calculations of the average strength of cation−π interactions in globular proteins yield values of −3.3 ± 1.5 and −2.9 ± 1.4 kcal/mol for cation−π pairs involving Lys and Arg, respectively (*7*). In contrast, experimental studies of cation−π interactions in α-helical peptides showed that no additional stability is provided to the α-helix by *i*, *i* + 4 Trp-Lys and Phe-Arg pairs (*12*) although *i*, *i* + 4 Trp-Arg pairs provide −0.4 kcal/mol of stabilization (*13*). Another study showed that the interactions of Phe with Lys or Arg are found to be weakly stabilizing (−0.1 to −0.2 kcal/mol) and do not depend on their relative orientation in the α-helix (*14*). Cation−π interactions have also been studied in the context of a β-hairpin. It was found that cation−π interactions stabilize the hairpin between −0.2 and −0.5 kcal/mol (*15*). Thus the magnitude of cation−π interactions obtained from experimental studies in model α-helix and β-hairpin peptides is found to be considerably smaller than calculated estimates (*7*).

Given the potential impact of cation−π interactions on the stability of globular proteins, we have attempted to determine the magnitude of cation−π interactions by disrupting specific cation−π interactions present in four different proteins: LIVBP,[1] MBP, RBP, and Trx. The first three proteins are relatively large (36.77, 40.70, and 28.47 kDa, respectively), monomeric, two-domain proteins found in the periplasm of *Escherichia coli.* They are involved in binding

† This work was supported by grants from the Department of Biotechnology and Department of Science and Technology, Government of India, to R.V.

* Address correspondence to this author at the Indian Institute of Science. E-mail: varadar@mbu.iisc.ernet.in. Phone: 91-80-22932612. Fax: 91-80-23600535.

‡ Indian Institute of Science.

§ Jawaharlal Nehru Center for Advanced Scientific Research.

10.1021/bi061275f CCC: $33.50
Published on Web 11/16/2006

and transport of leucine/isoleucine/valine, maltose, and ribose, respectively. Trx is a 108 amino acid, cytoplasmic *E. coli* disulfide oxidoreductase. The CaPTURE (cation−π trends using realistic electrostatics) program (*7*) was used to identify cation−π pairs present in the above proteins. The cationic amino acid residue of the cation−π pair was replaced with Gln and Met. In a separate series of experiments, the aromatic amino acid in each cation−π pair was replaced by Leu. Stabilities of WT and mutant proteins were characterized by thermal as well as chemical denaturation. The free energy ($\Delta G°$) obtained for cation−π interactions was found to range from +1.1 to −1.9 kcal/mol (average value −0.4 kcal/mol) at 298 K and +0.7 to −2.6 kcal/mol (average value −1.1 kcal/mol) at the T_m of each WT.

MATERIALS AND METHODS

Mutagenesis, Expression, and Protein Purification. All mutants were constructed by site-directed mutagenesis following the Stratagene Quik-Change protocol as described previously (*16*). All mutations were confirmed by DNA sequencing.

Plasmid pJSty expressing LIVBP under the control of the T7 promoter was used for mutagenesis of LIVBP. K248Q, F332L, and K248M mutants were constructed. WT and mutant proteins were expressed in the BL21(DE3) *E. coli* bacterial strain. Cells were grown in LB medium containing 100 mg/L ampicillin at 37 °C and induced with 0.1 mM IPTG at an OD_{600} of 0.8. After 6 h incubation at 37 °C, cells were pelleted at 6000 rpm. Following osmotic shock (*17*) the protein was further purified by ion-exchange chromatography on a Q-Sepharose fast-flow column using a 0−0.4 M NaCl gradient in 10 mM Tris buffer, pH 8 at 4 °C.

The malE (MBP) gene cloned in the vector pMALp2MBP (*18*) was used as a template for mutagenesis of MBP. K170Q, Y167L, and K170M mutants were constructed. WT and mutant proteins were expressed in the *E. coli* strains DH5α and Pop-6590 (ΔmalE), respectively, by inducing the cell culture with 0.1 mM IPTG (*19*, *20*). Proteins were isolated, following osmotic shock as described previously (*20*).

The rbsB gene (RBP) cloned in plasmid pCMB1 was used as the template for mutagenesis of RBP. K243Q, Y261L, and K243M mutants were constructed. Mutant and WT proteins were expressed in the RBP deletion strain Mri7 (Δ*rbsB*) (*21*) and DH5α, respectively. Protein was isolated and purified by a similar procedure as described above for LIVBP.

The TrxA gene cloned in vector pET20b(+) under control of the T7 promoter was used as the template to construct K57Q, W28L, and K57M mutants. WT and mutant genes present in the plasmid pET20bTrx were expressed in strain BL21(DE3) without induction as this plasmid showed leaky expression. Following chloroform shock, WT and mutant Trx proteins were isolated as described previously (*22*).

Protein purity was assessed by Coomassie staining following SDS−PAGE. All of the proteins were >95% pure. Protein concentrations were estimated using extinction coefficients of 35600, 65370, 4350, and 13700 M^{-1} cm^{-1} at 280 nm for LIVBP, MBP, RBP, and Trx, respectively. The extinction coefficients of MBP and Trx were identical to those described previously (*20*, *23*), and those for LIVBP and RBP were calculated as described previously (*24*). RBP lacks Trp residues and therefore has a small extinction coefficient.

CD and Fluorescence Measurement. CD spectra of WT LIVBP, MBP, and RBP and their mutant proteins were acquired in buffer CGH5 (citrate, HEPES, and glycine, 5 mM each) at pH 7. For WT and mutant MBP proteins, spectra were also acquired in CGH5 buffer containing 10 mM maltose. Phosphate buffer (10 mM), pH 7, was used for WT and mutants of Trx as described previously (*25*). All CD spectra were recorded on a Jasco J-715 CD spectrometer. Wavelength scans from 200 to 250 nm for 5−8 μM proteins were performed in a 0.1 cm path length cuvette using a slit width of 1 nm and a scan rate of 20 nm/min.

Isothermal Equilibrium Unfolding Studies of LIVBP, MBP, RBP, and Trx. Isothermal urea denaturation studies of LIVBP, MBP, and RBP and their mutants were carried out in CGH10 buffer containing 150 mM NaCl at pH 7, 298 K, as described previously (*20*, *26*). Maltose (10 mM) was also included in the case of maltose-bound MBP (MBP/maltose). Isothermal GdmCl denaturation studies of Trx and its mutants were carried out in 50 mM phosphate buffer at pH 7, 298 K, as described previously (*25*). Denaturation was monitored using fluorescence on a Fluoro-Max3 fluorometer except for W28L Trx where denaturation was monitored by CD at 222 nm. W28L does not show a large change in fluorescence intensity upon unfolding. Protein concentrations of 3, 0.5, 0.5, 8, and 5 μM for LIVBP, MBP, MBP/maltose, RBP, and Trx were used, respectively. All proteins were incubated at 25 °C for 5 h. This time was sufficient to attain equilibrium as monitored by the time independence of the fluorescence intensity. Longer incubation times (up to 10 h) did not result in any changes in the measured stability parameters. The denaturant concentration was estimated by refractive index measurements. Unfolding was monitored by measuring fluorescence at 323, 337, 350, 303, and 338 nm for LIVBP, MBP, MBP/maltose, RBP, and Trx, respectively, and all of the proteins were excited at 280 nm. Values of the parameters $\Delta G°$ and *m* were estimated according to the linear free energy model as described previously (*19*, *27*). All of the data was analyzed using Sigma Plot.

Thermal Denaturation. Thermal denaturation for WT and mutant proteins was carried out using the Microcal VP-DSC. DSC measurements were carried out as a function of pH in CGH10 buffer, in the pH range 6−10, using protein concentrations of 0.2−0.5 mg/mL. Protein solutions used for the DSC study were dialyzed against CGH10 at pH 7 and degassed before being loaded into the microcalorimeter. The pH was adjusted manually before degassing. A scan rate of 90 °C/h was used for MBP, MBP/maltose, RBP, and LIVBP and 60 °C/h for Trx as described previously (*20*, *25*). DSC scans were carried out from 25 to 85 °C for LIVBP, MBP, and RBP and from 25 to 110 °C for Trx and MBP/maltose. For all proteins, the reversibility of thermal unfolding was confirmed by carrying out a rescan at each pH before the

[1] Abbreviations: LIVBP, leucine−isoleucine−valine binding protein; MBP, maltose binding protein; RBP, ribose binding protein; Trx, *Escherichia coli* thioredoxin; GdmCl, guanidinium chloride; DSC, differential scanning calorimetry; CGH10, 10 mM citrate, 10 mM glycine, and 10 mM HEPES; WT, wild type; CaPTURE, cation−π trends using realistic electrostatics.

Table 1: Cation−π Interactions Detected in the Structure of LIVBP, MBP, MBP/Maltose, RBP, and Trx Using the Program CaPTURE (*7*)[a]

protein (PDB ID)	cation amino acid	aromatic amino acid	*E*(elec) (kcal/mol)	*E*(vdw) (kcal/mol)
LIVBP	Arg109	Tyr111	−2.0	−2.3
(2liv)	Arg188	Phe171	−5.5	−3.6
	Lys248	**Phe332**	**−4.9**	**−1.4**
MBP	**Lys170**	**Tyr167**	**−3.2**	**−1.0**
(1omp)	Lys297	Trp17	−2.1	−0.6
	Arg316	Trp232	−4.5	−2.5
MBP/maltose	Arg316	Trp232	−4.6	−3.2
(1anf)	**Lys170**	**Tyr167**	**−1.3**	**−1.0**
	Lys15	Trp62	−2.2	−0.1
	Lys15	Trp230	−4.8	−1.0
RBP	Arg141	Phe214	−4.07	−3.1
(1urp)	**Lys243**	**Tyr261**	**−3.1**	**−1.0**
Trx	**Lys57**	**Trp28**	**−2.7**	**−0.6**
(2trx)				

[a] Cation−π pairs in bold font were selected for further characterization because the positively charged amino group did not form extensive additional electrostatic interactions with other residues. Electrostatic (elec) and van der Waals (vdw) components of the calculated cation−π interaction energy are shown.

sample was removed from the calorimeter. DSC data were fit to a two-state unfolding with baseline subtraction model using the Origin DSC software provided by Microcal Inc.

RESULTS

Identification of Cation−π Interactions. LIVBP, MBP, MBP/maltose, RBP, and Trx have been used in the present study as model systems for studying the contribution of cation−π interactions to protein stability, because these proteins can be expressed to high levels in *E. coli* and showed reversible thermal and chemical denaturation, and crystal structures of the WT protein are available.

The CaPTURE program (*7*) (http://capture.caltech.edu/) was used for identifying cation−π interactions. Five Arg and seven Lys aromatic pairs were identified as cation−π interacting pairs in the LIVBP, MBP, MBP/maltose, RBP, and Trx structures. The results are shown in Table 1. The contribution of cation−π interactions to protein stability was studied by mutating the cationic residue from the cation−π pair present in the WT protein, thereby leading to disruption of the cation−π interaction which should lead to destabilization of mutant proteins. The cationic residues were found to be more exposed than the corresponding partner aromatic residues. Hence mutation of the cationic residues would be expected to result primarily in loss of the cation−π interaction alone and not in alteration of packing interactions with nearby residues or in changes in protein structure upon mutation. Cation−π pairs (Lys248-Phe332, LIVBP; Lys170-Tyr167, MBP; Lys170-Tyr167, MBP/maltose; Lys243-Tyr261, RBP; Lys57-Trp28, Trx) were selected for mutation. In all of these cases, the charged group of the cationic residue is not involved in extensive electrostatic/hydrogen-bonding interactions with the surrounding residues (Figure 1). Each such cationic residue was replaced with Gln and Met to study the effect of these mutations on protein stability. It was of interest to compare the stabilities of identical mutants in the MBP unbound and maltose-bound structures since the calculated cation−π interaction energy is appreciably weaker in the maltose-bound structure. In order to study the effect of altering the aromatic amino acid, each of the aromatic partners was mutated to Leu. As discussed above, changes in stability in these mutants will be due to the changes in packing interactions as well as loss of the cation−π interaction. Unfortunately, there is no naturally occurring aliphatic isostere or near isostere for any of the aromatic amino acids.

Characterization of WT and Mutant Proteins. All proteins were purified and found to be >95% pure by SDS−PAGE. Approximate yields of purified WT and mutant proteins were 20, 25, 40, and 90 mg/L for LIVBP, MBP, RBP, and Trx, respectively. Mutant proteins showed fluorescence (data not shown) and far-UV CD spectra similar to the corresponding WT (Figure 2) with exception of the W28L Trx mutant, which shows reduced fluorescence. Hence there are unlikely to be major changes in the structure of any of the mutant proteins.

Chemical Denaturation Studies. All mutants were expected to be destabilized due to the loss of cation−π interactions. Chemical denaturation studies of mutant and WT proteins were carried out using either urea (for LIVBP, MBP, MBP/maltose, and RBP) or GdmCl (for Trx) (*25*). Urea was used for denaturation of LIVBP, MBP, MBP/maltose, and RBP because the transition with GdmCl is highly cooperative for these relatively large proteins (*26*, *28*). Therefore, it is technically difficult to obtain a large number of data points in the transition region. In addition, GdmCl may screen out electrostatic interactions. For Trx, it was not possible to carry out urea denaturation as the protein only starts to denature at urea concentrations over 6 M and no unfolded baseline could be obtained. Denaturation was monitored using fluorescence spectroscopy or CD spectroscopy (for W28L Trx) as described in Materials and Methods. Data were fit to a two-state unfolding model. The free energies of unfolding at zero denaturant were determined using linear extrapolation as described previously (*29*). Denaturation of MBP, Trx, and RBP had been shown previously to be two state by coincidence of melts monitored by fluorescence and far-UV CD (*20*, *25*, *26*). Denaturation of LIVBP was also found to be two state by the same criterion. Due to the highly cooperative nature of the unfolding transition, the *m* value obtained from an individual fit was not very reliable. Hence a global fit was conducted by constraining the *m* value for mutants and the respective WT to be identical as described previously (*19*). The global fits for LIVBP, MBP, MBP/maltose, RBP, and Trx were conducted separately, and the results are summarized in Figure 3 and Table 2. K243M and K57M mutants of RBP and Trx, respectively, were found to be more stable than the corresponding WT. The remaining 13 mutants were found to be less stable than the corresponding WT. In addition, all the Gln and aromatic → Leu mutants were less stable than the Met mutants with respect to chemical denaturation. Values of $\Delta\Delta G°$ [$\Delta G°$(mutant) − $\Delta G°$(WT)] for chemical denaturation ranged from −0.3 to −2.6 kcal/mol for Gln mutants, +1.1 to −1.9 kcal/mol for Met, and −0.3 to −4.4 kcal/mol for the aromatic → Leu mutants at 298 K, pH 7.0.

Thermal Denaturation Studies. DSC was used to characterize the thermal stabilities for all proteins in the pH range 6.0−10.0. DSC scans for all proteins were reversible, and the data fit well to a two-state model. At the T_m of unfolding, 50% of the molecules are folded and $\Delta G°(T_m) = 0$. The results are summarized in Table 3, and the DSC data at pH

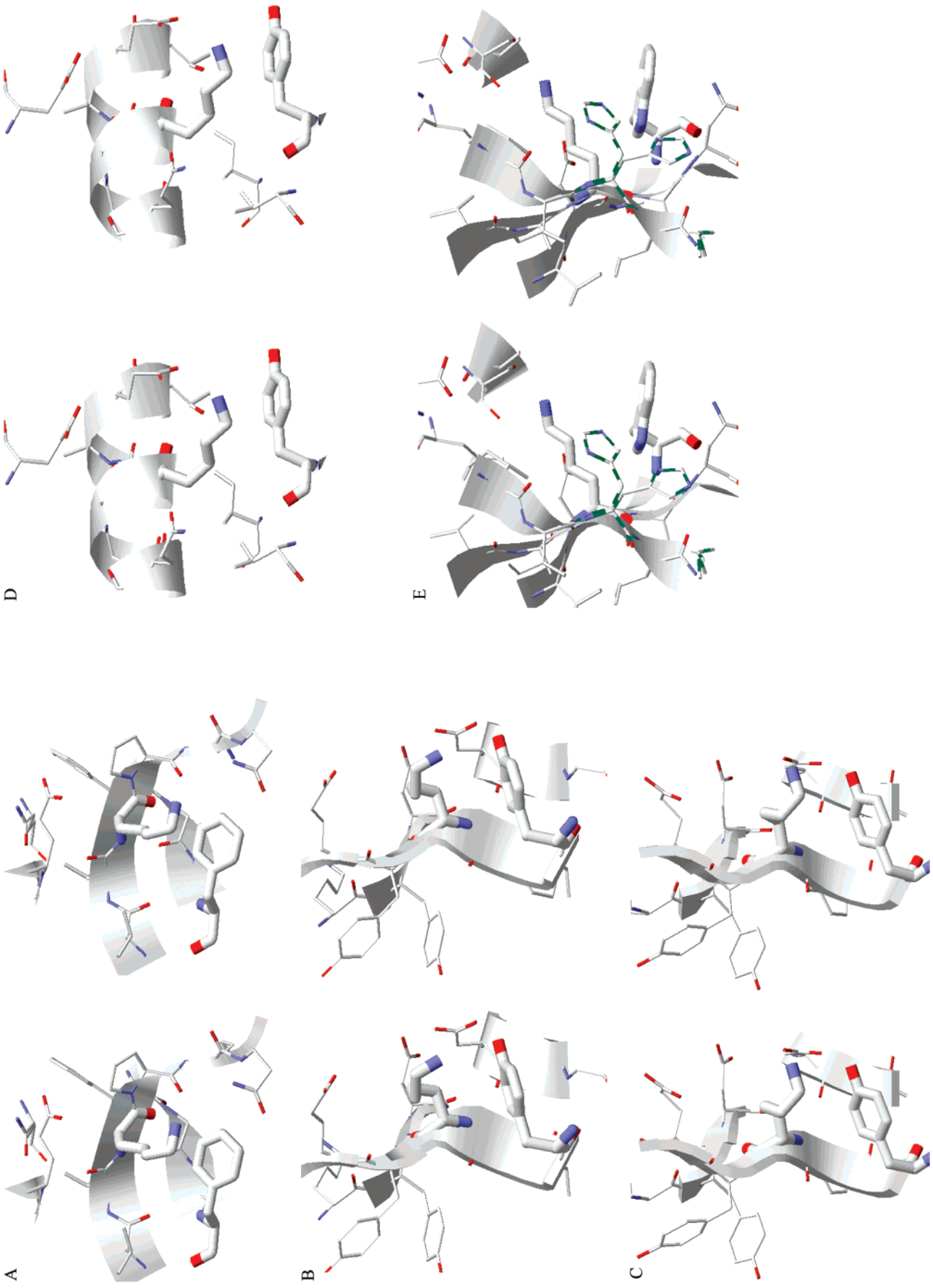

FIGURE 1: Stereoviews of the location of cation−π pairs selected for mutation in the structures of WT (A) LIVBP, (B) MBP, (C) MBP/maltose, (D) RBP, and (E) Trx. Residues comprising the cation−π pair are shown in thick lines. Nitrogen atoms are colored blue and oxygen red. The figure was generated using the program RasTop (45).

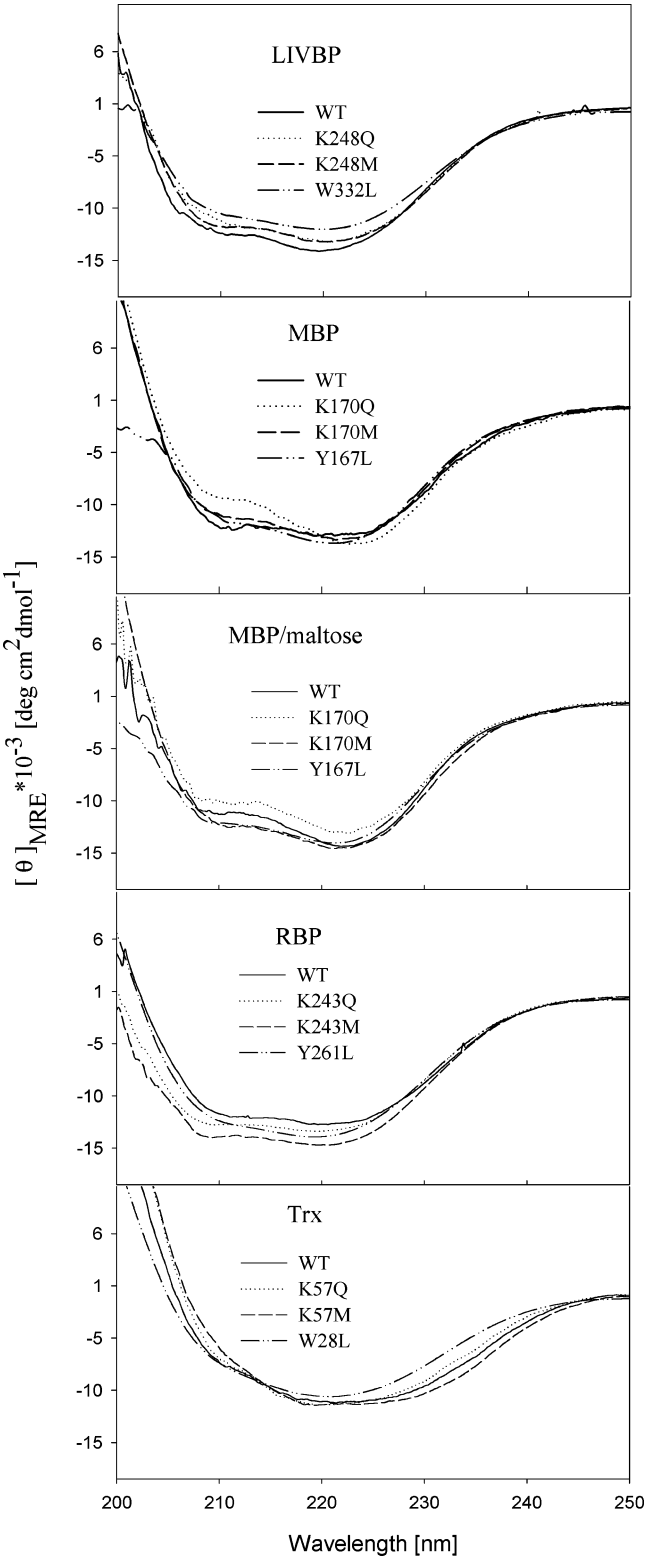

FIGURE 2: Far-UV CD spectra for WT and mutants of LIVBP, MBP, RBP, and Trx at pH 7 and 298 K.

7 are shown in Figure 4. All of the mutants showed significant decreases in T_m except the K243M and K57M mutants of RBP and Trx, which showed similar average T_m to the corresponding WT. The significance of changes in T_m was assessed by carrying out a paired *t*-test for WT and mutant T_m values as a function of pH (*19*) (Table 3). Values of ΔC_p for each protein were estimated from the slope of the linear dependence of $\Delta H°(T_m)$ upon T_m. Values of ΔC_p

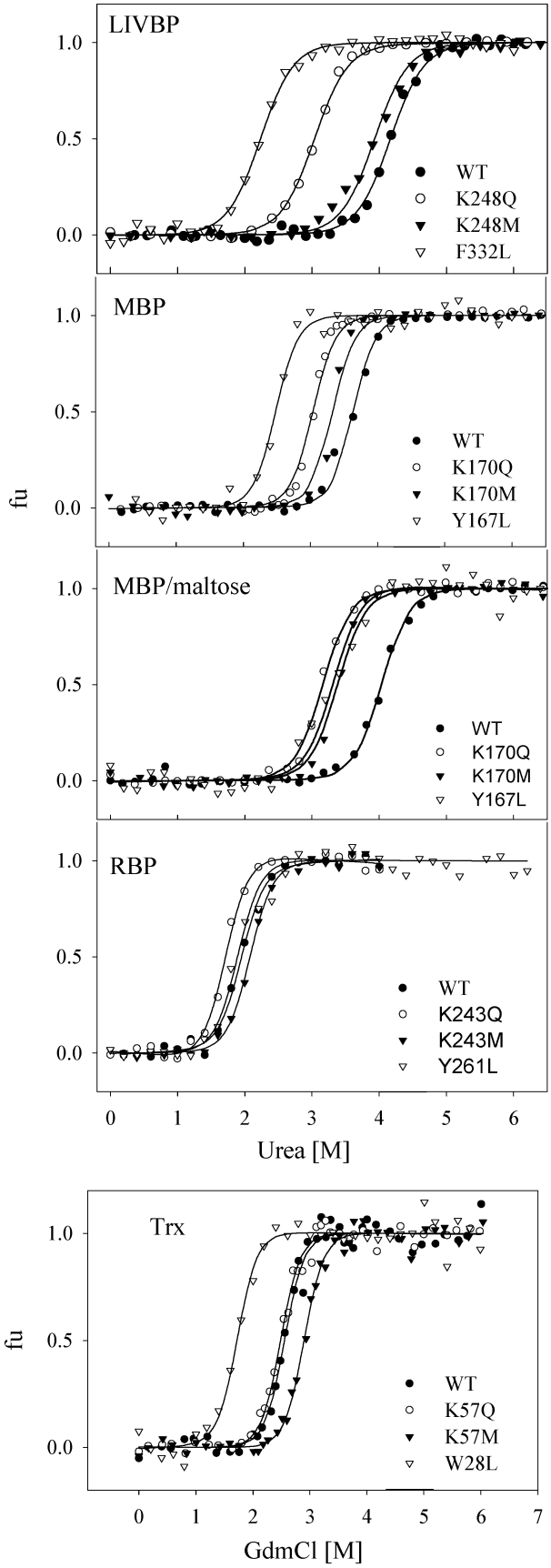

FIGURE 3: Isothermal chemical denaturation curves at pH 7, 298 K, for WT and mutants of LIVBP, MBP, MBP/maltose, RBP, and Trx. Protein denaturation was monitored by protein fluorescence as described in the text. The fraction of unfolded protein (fu) is plotted as a function of denaturant concentration.

Table 2: Unfolding Thermodynamic Parameters Obtained from Isothermal Denaturation Studies Done at pH 7, 298 K, for WT and Mutants of LIVBP, MBP, MBP/Maltose, RBP, and Trx[a]

protein	$\Delta G°$ (kcal/mol)	m (kcal mol^{-1} M^{-1})	C_m (M)	$\Delta\Delta G°$ (kcal/mol)	ΔC_m (M)
LIVBP					
WT	9.8 ± 0.4	−2.4 ± 0.1	4.0		
K248Q	7.2 ± 0.2	−2.4 ± 0.1		−2.6 ± 0.4	−1.1
K248M	9.3 ± 0.3	−2.4 ± 0.1		−0.5 ± 0.5	−0.2
F332L	5.4 ± 0.1	2.4 ± 0.1		−4.4 ± 0.1	−1.7
MBP					
WT	12.6 ± 0.3	−3.5 ± 0.1	3.6		
K170Q	10.5 ± 0.2	−3.5 ± 0.1		−2.1 ± 0.4	−0.6
K170M	11.5 ± 0.2	−3.5 ± 0.1		−1.1 ± 0.4	−0.3
Y167L	8.7 ± 0.1	−3.5 ± 0.1		−3.9 ± 0.1	−1.1
MBP/maltose					
WT	11.4 ± 0.3	−2.8 ± 0.1	4.0		
K170Q	8.9 ± 0.2	−2.8 ± 0.1		−2.5 ± 0.4	−0.9
K170M	9.5 ± 0.2	−2.8 ± 0.1		−1.9 ± 0.4	−0.7
Y167L/maltose	9.3 ± 0.1	−2.8 ± 0.1		−2.1 ± 0.1	−0.7
RBP					
WT	6.7 ± 0.5	−3.4 ± 0.2	2.0		
K243Q	5.9 ± 0.4	−3.4 ± 0.2		−0.8 ± 0.5	−0.2
K243M	7.1 ± 0.5	−3.4 ± 0.2		0.4 ± 0.6	0.1
Y261L	6.4 ± 0.2	−3.4 ± 0.2		−0.3 ± 0.1	−0.1
Trx					
WT	8.7 ± 0.3	−3.4 ± 0.1	2.6		
K57Q	8.4 ± 0.3	−3.4 ± 0.1		−0.3 ± 0.4	−0.1
K57M	9.8 ± 0.4	−3.4 ± 0.1		1.1 ± 0.5	0.3
W28L	5.9 ± 0.2	−3.4 ± 0.1		−2.8 ± 0.1	−0.9

[a] $\Delta\Delta G° = \Delta G°$(mutant) − $\Delta G°$(WT).

for WT proteins were found to be 5.6 ± 0.6, 6.0 ± 1.2, 5.4 ± 1.9, 4.5 ± 0.2, and 1.2 ± 0.1 kcal mol^{-1} K^{-1} for LIVBP, MBP, MBP/maltose, RBP, and Trx, respectively. Mutant proteins had ΔC_p values approximately similar to that of the corresponding WT. To compare WT and mutant stabilities at a common temperature, the measured values of $\Delta H°(T_m)$ and $\Delta S(T_m)$ were extrapolated to a common reference temperature (T_m of WT at pH 7) using the measured values of ΔC_p as described previously (*25*). For WT and mutant LIVBP, MBP, MBP/maltose, RBP, and Trx the reference temperature was chosen to be 340.15, 337.75, 348.45, 336.15, and 360.95 K (the T_m of each WT protein), respectively. Values of changes in thermodynamic parameters at the reference temperature for each mutant, relative to the corresponding WT, are summarized in Table 4. These results are qualitatively in agreement with the isothermal denaturation studies. Values of $\Delta\Delta G°(T_m)$ ranged from −0.8 to −2.9 kcal/mol for Gln mutants, +0.7 to −2.6 kcal/mol for Met mutants, and −0.3 to −4.4 kcal/mol for aromatic → Leu mutants at pH 7.0. On average, the magnitude of destabilization is higher at the T_m than at room temperature for the Met mutants.

DISCUSSION

Previous Studies. Cation−π interactions are a common feature of protein structures with an average occurrence of one cation−π interaction in 77 residues (*7*). It has been explicitly demonstrated in several (*2*, *7*) studies that when a cationic side chain (Arg, Lys, or His) is located close to an aromatic side chain (Phe, Tyr, or Trp), the geometry is biased toward a favorable cation−π interaction. These interactions are dominated by the electrostatic component (*30*). Since the CH_2 directly adjacent to the positively charged groups of Lys or Arg carries substantial positive charge, proximity of such a CH_2 with aromatic side chains is considered to contribute to the cation−π interaction (*30*). Although the neutral nitrogen-containing side chains Asn and Gln also interact with aromatic rings, such amino−π interactions have previously been found to be weaker than cation−π interactions (*30*). The average magnitude of cation−π interactions in globular proteins was calculated to be approximately −3.3 ± 1.5 kcal/mol (Lys−aromatic residues) and −2.9 ± 1.4 kcal/mol (Arg−aromatic residues).

In contrast, previous studies with synthetic peptides suggest that cation−π interactions contribute −0.3 to −0.7 kcal/mol to stability (*13*, *31*−*33*). Although there have been several attempts to experimentally quantitate cation−π interactions in peptides, there are far fewer such studies in globular proteins. In one instance, it was shown that replacement of a buried Arg (that was part of a cation−π pair) with Met resulted in conversion of the native protein to a molten globule like state (*34*). However, buried charged residues are rarely found in protein structures (*35*), and consequently, most cation−π interactions occur at surface-exposed sites. In the present study we have therefore attempted to quantitate strengths of cation−π interactions at surface sites in proteins. Since globular proteins are more rigid and have different dielectric properties than peptides, it is possible that cation−π interaction strengths may be quantitatively different in peptides and proteins.

Amino−π Interaction Estimates. The CaPTURE algorithm (*7*) (http://capture.caltech.edu/) was used to identify cation−π interactions because the energies calculated using this algorithm can be compared with experiment, in contrast to geometry-based methods. Identified cation−π pairs are shown in Table 1. In the case of all the Arg−aromatic pairs, the side chains of the Arg residues were also involved in extensive hydrogen-bonding interactions with surrounding residues. In addition, it is difficult to find a suitable approximately isosteric replacement for Arg. Hence Arg−aromatic interactions could not be studied. This work involved mutations of both the Lys and aromatic residues involved in cation−π interactions (Lys-Phe, Lys-Tyr, and Lys-Trp) (Figure 1). The Lys side chain ($-CH_2-CH_2-CH_2-CH_2-NH_3^+$) was replaced by Gln ($CH_2-CH_2CONH_2$) and Met ($-CH_2-CH_2-S-CH_3$) side chains in each of the cation−π pairs. The Gln side chain has a polar $CONH_2$ group capable of hydrogen bonding and some degree of electrostatic interaction. However, it has two fewer hydrophobic $-CH_2$ groups relative to Lys. Asn/Gln amino−π interactions involving Asn/Gln and aromatic rings have also been thought to be stabilizing (*36*). The difference in stability between Gln mutants and the corresponding WT will reflect on the contribution of the two terminal hydrophobic $-CH_2$ groups of Lys to protein stabilization as well as on the relative electrostatic contributions of a positively charged amino versus a polar, uncharged amide group interaction with the aromatic ring. Values of $\Delta\Delta G°$ of Gln mutants varied from −0.3 to −2.6 kcal/mol at 298 K, confirming that amino−π interactions are weaker than cation−π ones.

Aromatic Amino Acid Replacements. The aromatic residue in each case was replaced with the aliphatic residue Leu. Leu has a similar volume (168 vs 200 Å^3) to Phe (*37*) and also has a γ-branched carbon. However, the overall shape of the Leu side chain is different from the planar aromatic ring. Hence replacement of the aromatic amino acid in the

Table 3: Thermodynamic Parameters for the Thermal Unfolding of WT and Mutants of LIVBP, MBP, MBP/10 mM Maltose, RBP, and Trx as a Function of pH Obtained from DSC[a]

protein	pH	T_m[b] (°C)	ΔH[b] (kcal/mol)	ΔT_m (°C)	average ΔT_m (°C)	P value[c]
LIVBP						
WT	6.0	68.9	177			
	6.5	68.9	172			
	7.0	67.0	164			
	7.5	67.0	162			
	8.0	64.3	139			
	8.5	63.2	148			
	9.0	60.2	125			
K248Q	6.0	63.5	163	−5.4		
	6.5	62.9	154	−6.0		
	7.0	61.4	137	−5.6		
	7.5	59.9	135	−7.1		
	8.0	58.7	129	−5.6		
	8.5	55.9	122	−7.3		
	9.0	54.1	110	−6.1	−6.2	6.4e−7
K248M	6.0	65.2	171	−3.7		
	6.5	65.2	165	−3.7		
	7.0	63.8	158	−3.2		
	7.5	61.7	138	−5.3		
	8.0	60.6	130	−3.7		
	8.5	56.8	112	−6.4		
	9.0	55.2	117	−5.0	−4.4	5.4e−5
F332L	7.0	62.4	119	−4.6		
	8.0	59.8	151	−4.5		
	9.0	54.2	121	−6.0	−5.0	5.1e−4
MBP						
WT	6.5	65.3	238			
	7.0	64.6	217			
	7.4	63.1	207			
	8.0	61.4	185			
	8.5	60.5	178			
	9.0	58.6	204			
	9.5	56.4	178			
K170Q	6.5	62.0	218	−3.3		
	7.0	61.0.	213	−3.6		
	7.4	60.9	201	−2.2		
	8.0	58.9	195	−2.5		
	8.5	57.5	192	−3.0		
	9.0	56.1	184	−2.5		
	9.5	53.6	161	−2.8	−2.8	4.0e−6
K170M	6.5	65.8	223	0.5		
	7.0	62.2	216	−2.4		
	7.4	61.1	202	−2.0		
	8.0	58.6	189	−2.8		
	8.5	57.6	173	−2.9		
	9.0	56.9	179	−1.7		
	9.5	54.6	156	−1.8	−1.9	4.9e−3
Y167L	7.0	62.0	161	−2.6		
	8.0	58.3	145	−3.1		
	9.0	55.7	134	−2.9	−2.9	2.61e−3
MBP/maltose						
WT	6.5	75.8	220			
	7.0	75.3	225			
	7.4	75.0	214			
	8.0	74.3	200			
	8.5	72.8	199			
	9.0	71.2	196			
	9.5	70.6	188			
K170Q/maltose	6.5	71.6	227	−4.2		
	7.0	71.1	220	−4.2		
	7.4	70.2	219	−4.8		
	8.0	69.2	215	−5.1		
	8.5	69.3	205	−3.5		
	9.0	68.3	207	−2.9		
	9.5	67.4	194	−3.2	−4.0	1.3e−5
K170M/maltose	6.5	72.3	223	−3.5		
	7.0	71.4	220	−3.9		
	7.4	70.9	216	−4.1		
	8.0	70.3	202	−4.0		
	8.5	69.3	197	−3.5		
	9.0	68.7	192	2.5		
	9.5	67.5	196	−3.1	−3.5	3.2e−6
Y167L/maltose	7.0	69.3	228	−6.0		
	8.0	67.3	194	−7.0		
	9.0	65.4	181	−5.9	−6.3	3.0e−3
RBP						
WT	5	64.2	112			
	6	63.7	108			
	7	63.0	106			
	8	62.2	102			
	9	61.0	98			
	10	60.0	92			
K243Q	5	61.1	96	−3.1		
	6	60.4	91	−3.3		
	7	59.6	89	−3.4		
	8	58.1	88	−4.1		
	9	57.4	82	−3.6		
	10	55.9	76	−4.1	−3.6	4.5e−6
K243M	5	64.2	95	0.0		
	6	63.8	91	0.1		
	7	62.0	89	−1.0		
	8	60.6	84	−1.6		
	9	60.1	81	−0.9		
	10	59.7	76	−0.3	−0.6	0.071
Y261L	7.0	61.5	95	−1.5		
	8.0	59.1	100	−3.1		
	9.0	58.1	93	−2.9	−2.5	0.04
Trx						
WT	6	88.6	122			
	7	87.8	119			
	8	86.3	118			
	9	85.6	117			
	10	81.0	112			
K57Q	6	87.9	118	−0.7		
	7	85.4	112	−2.4		
	8	82.6	107	−3.7		
	9	80.5	103	−5.1		
	10	77.2	98	−3.8	−3.1	0.013
K57M	6	91.7	119	3.1		
	7	90.1	112	2.3		
	8	86.8	104	0.5		
	9	84.6	104	−1.0		
	10	80.3	96	−0.7	0.8	0.358
W28L	7.0	76.3	103	−11.5		
	8.0	73.6	100	−12.7		
	9.0	72.6	96	−13.0	−12.4	1.4e−3

[a] All DSC data were fit to a two-state model. [b] Approximate errors in T_m and ΔH are 0.1 °C and 5%, respectively. [c] P value for paired t-test to assess statistical significance of the difference in the WT and mutant T_m values. P values less than or equal to 0.1 are considered significant.

cation−π pair with Leu will result in disruption of local packing as well as loss of the cation−π interaction. Indeed, with the exception of the RBP Y261L mutant, all of the other aromatic → Leu replacements resulted in a relatively large destabilization of −1.8 to −4.4 kcal/mol (Table 5). There was no clear pattern to the temperature dependence of $\Delta\Delta G°$

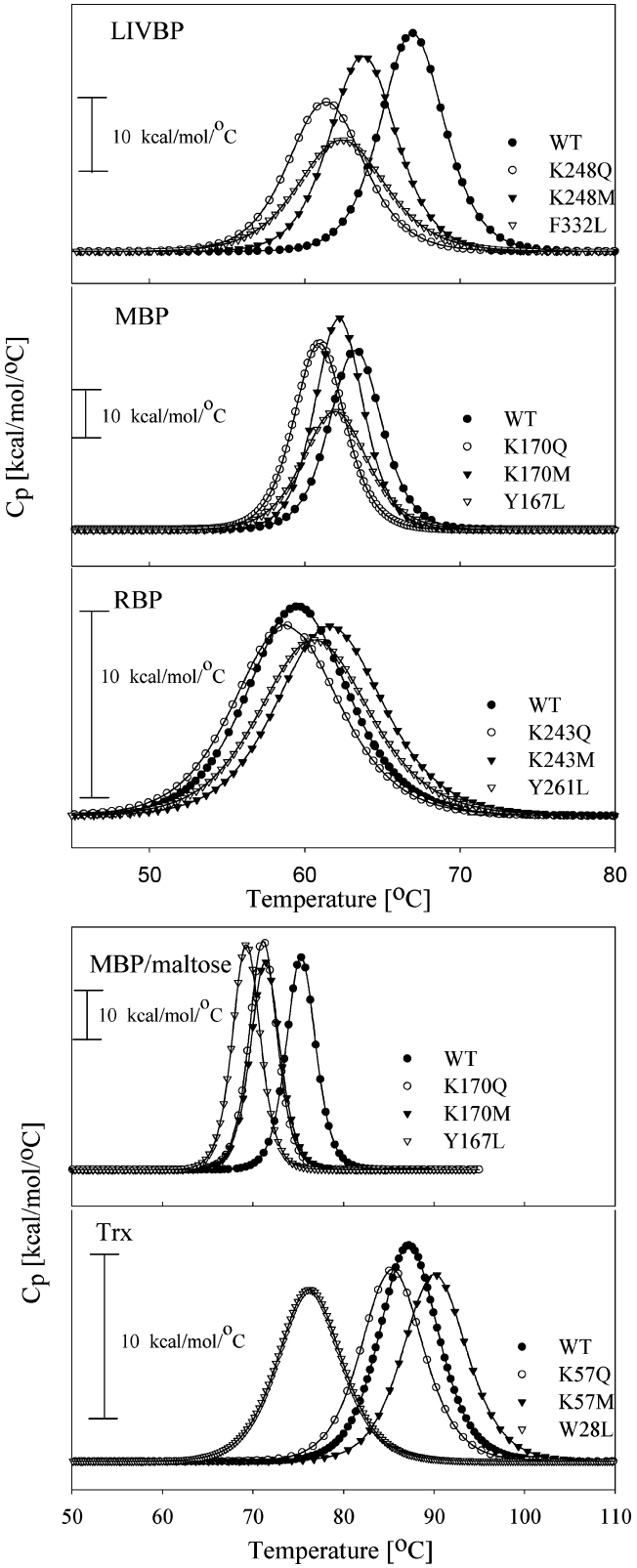

FIGURE 4: Baseline subtracted DSC scans for WT and mutants of LIVBP, MBP, RBP, MBP/maltose, and Trx at pH 7. Data points are shown as symbols, and two-state fits to the data are shown as thin solid lines.

for this class of mutants. In addition to the shape differences between the aromatic side chain and Leu, in three of the four proteins, the Tyr or Trp aromatic amino acid side chain of the cation−π pair is also involved in hydrogen-bonding interactions. In LIVBP, although the F332 side chain cannot

Table 4: Changes in Thermodynamic Unfolding Parameters at pH 7 for Mutants of LIVBP, MBP, MBP/Maltose, RBP, and Trx, Respectively, Relative to Their Corresponding WT at the Reference Temperature[a]

protein	$\Delta\Delta H°$ (kcal/mol)	$\Delta\Delta S$ (cal mol^{-1} K^{-1})	$T\Delta\Delta S$ (kcal/mol)	$\Delta\Delta G°$ (kcal/mol)	ΔT_m[b] (°C)
LIVBP					
K248Q	0.7	9.6	3.3	−2.5	−5.6
K248M	12.1	40.3	13.7	−1.6	−3.2
F332L	−19.1	−50.9	−17.3	−1.8	−5.0
MBP					
K170Q	17.9	60.2	20.3	−2.4	−3.6
K170M	13.9	45.8	15.5	−1.6	−2.4
Y167L	−42.0	−120.6	−40.7	−1.3	−2.9
MBP/maltose					
K170Q	24.2	77.8	27.1	−2.9	−4.2
K170M	22.3	71.5	24.9	−2.6	−3.9
Y167L	39.1	124.5	43.4	−4.3	−6.3
RBP					
K243Q	−5.2	−12.7	−4.3	−1.0	−3.4
K243M	−13.5	−39.5	−13.3	−0.3	−1.0
Y261L	−4.3	−11.5	−3.9	−0.4	−2.5
Trx					
K57Q	−2.5	−4.9	−1.8	−0.8	−2.4
K57M	−11.3	−33.2	−12	0.7	2.3
W28L	−2.2	4.0	1.5	−3.7	−12.4

[a] For all mutants of LIVBP, MBP, MBP/maltose, RBP, and Trx the reference temperature was chosen to be 340.15, 337.75, 348.45, 336.15, and 360.95 K (T_m of the corresponding WT at pH 7), respectively. [b] Average ΔT_m values from Table 3.

be involved in hydrogen bonding, it is quite buried and tightly packed against surrounding residues (Table 5, Figure 5). In MBP Y167 OH forms a tertiary hydrogen bond with the side chain of D180 that appears to be involved in stabilizing the interaction between two β-strands. Y167 is also tightly packed against surrounding residues (Figure 5). This interaction is present in both maltose-free and -bound states. In RBP Y261 OH is involved in a localized hydrogen bond with the main chain amide of Q258. Loss of this hydrogen bond is not expected to be destabilizing as the Q258 residue is solvent exposed and the amide can form a hydrogen bond with solvent. Also, Y261 in RBP is not as tightly packed as Y167 in MBP. This is consistent with the lack of destabilization observed in Y261 RBP. In Trx the indole ring of W28 is buried, tightly packed, and forms a hydrogen bond with a buried water molecule. Both the packing of the indole ring and this hydrogen bond would be disrupted in the W28L mutant. The above analysis supports the assertion that the observed destabilization in the aromatic → Leu mutants has significant contribution from loss of packing and hydrogen bond interactions and therefore cannot be used to quantitate the cation−π interaction.

Cation−π Interaction Estimates. In contrast to Gln, Met has an identical number of hydrophobic groups as Lys, except that one nonpolar CH_2 group is replaced by a nonpolar sulfur atom. In addition, Met lacks the positively charged $-NH_3^+$ group. The difference in stability between Met mutants and the corresponding WT should therefore be a measure of the electrostatic component of the cation−π interaction. Met mutants were found to be consistently more stable than the corresponding Gln mutants. We suggest that this is primarily because Met is a closer isostere of Lys than Gln and consequently will have better packing interactions with neighboring residues than Gln. Some crystallographic analyses have suggested that sulfur−aromatic interactions may

Table 5: Structural and Thermodynamic Parameters at Sites of Mutation in LIVBP, MBP, MBP/Maltose, RBP, and Trx

protein (cation−π pair)	E(electrostatic)[a] (kcal/mol)	% accessibility: cationic residue	% accessibility: aromatic residue	acceptor/ distance (Å)[b]	L mutants[c]: $\Delta\Delta G°$ (298 K)	L mutants[c]: $\Delta\Delta G°$ (T_m)	Q mutants[c]: $\Delta\Delta G°$ (298 K)	Q mutants[c]: $\Delta\Delta G°$ (T_m)	M mutants[c]: $\Delta\Delta G°$ (298 K)	M mutants[c]: $\Delta\Delta G°$ (T_m)
LIVBP (K248-F332)	−4.9	27.2	3.5	249 O/2.7	−4.4	−1.8	−2.6	−2.5	−0.5	−1.6
MBP (K170-Y167)	−3.2	39.4	28.8	180 OD2/3.7	−3.9	−1.3	−2.1	−2.4	−1.1	−1.6
MBP/maltose (K170-Y167)	−1.3	47.4	32.2	180 OD2/2.6	−2.1	−4.3	−2.5	−2.9	−1.9	−2.6
RBP (K243-Y261)	−3.1	33.0	22.3	246 OE1[d]/2.8	−0.3	−0.4	−0.8	−1.0	0.4	−0.3
Trx (K57-W28)	−2.7	20.3	24.5		−2.8	−3.7	−0.3	−0.8	1.1	0.7

[a] Calculated electrostatic energy values obtained from Table 1. [b] Identity and distance of closest potential H-bond acceptor/negative charge within 4 Å of the cation. [c] $\Delta\Delta G°$ (298 K) and $\Delta\Delta G°$ (T_m) values obtained from Tables 2 and 4, respectively. [d] This acceptor is also solvated by two additional water molecules.

be stabilizing (*38*, *39*). However, experimental thermodynamic studies in proteins (*40*, *41*) and peptides (*32*) find no difference in the interaction energetics of Met and the isosteric Nle with nearby aromatic residues. This suggests that Met−aromatic interactions are essentially hydrophobic in nature. The strength of the cation−π interaction was assessed by the value of the change in the free energy of unfolding when the Lys in a cation−π pair was replaced by Met [$\Delta\Delta G° = \Delta G°$(Met) − $\Delta G°$(WT)]. This ranged from +1.1 to −1.9 kcal/mol (average value −0.4 kcal/mol) at 298 K and +0.7 to −2.6 kcal/mol (average value −1.1 kcal/mol) at the T_m of each WT. At room temperature (Table 2) with the exception of MBP, in the other three proteins studied, the cation−π interaction energy [$\Delta\Delta G° = \Delta G°$(Met) − $\Delta G°$(WT)] is significantly different from the calculated values [E(electrostatic), Table 1] of −3 to −5 kcal/mol. The average difference $|\Delta G°_{expt} - \Delta G°_{calc}|_{av}$ is 2.9 kcal/mol. Even in the case of MBP, the cation−π interaction is predicted to be stronger in the MBP structure without maltose, but the measured value of $\Delta\Delta G°$ is higher for MBP/maltose. In two of the three proteins (RBP and Trx) values of $\Delta\Delta G°$ are actually positive, indicating that in these proteins the cation−π interaction is likely to be destabilizing at room temperature. The energetic contribution of the cation−π interaction at high temperature was evaluated through DSC studies (Tables 3 and 4). A comparison of $\Delta\Delta G°$ values for Met mutants in Tables 2 and 4 indicates a small increase in the strength of cation−π interactions at high temperature. Values of $\Delta\Delta G°$ in most cases are slightly more negative at high temperature, consistent with previous computational predictions regarding strengths of salt bridges at high temperatures (*42*).

Structural Analysis of Cation−π Interaction Sites. It has been previously reported that cation−π interactions showed a distance dependence of $1/r^n$, where n is <2 (*43*) and r is the distance between NZ or Cϵ of Lys and the centroid of the aromatic ring of the cation−π pair. However, there is no clear correlation of the measured $\Delta\Delta G°$ with these distances (data not shown). A summary of the structural characteristics of each site chosen for mutation as well as changes in the stability associated with each mutant is shown in Table 5. Although attempts were made to select Lys residues where the cation was involved solely in cation−π interactions, this was not always possible. In some of the cases, the cation is also involved in electrostatic interactions with negatively charged residues in its vicinity. Table 5 lists Asp and Glu residues where a carboxylate oxygen is within 5 Å of the NZ atom of the Lys residue participating in the cation−π interaction. A close analysis of the environment of the cation−π pair in each of the structures in Table 5 and Figure 1 shows that in all cases where the value of $\Delta\Delta G°$ for the Met mutant is negative there are additional stabilizing interactions (besides the cation−π) that are lost upon Lys → Met mutation. Hence the magnitude of $\Delta\Delta G°$ in these cases is likely to be an overestimate of the magnitude of the cation−π interaction energy. In the case of Trx where K57 is not involved in any other electrostatic interactions, the K57M mutant is clearly stabilized with respect to WT. In the case of RBP, although K243 is hydrogen bonded to the side chain of E246, the latter residue is also located close to two water molecules and another side chain, K250. Hence loss of the hydrogen bond with K243 is unlikely to be significantly destabilizing. Here, too, the K243M mutant is stabilized with respect to WT. In the case of MBP, visual comparison of the MBP and MBP/maltose structures (Figure 1) clearly demonstrates that the cation−π interaction is expected to be stronger in the former structure where the NZ atom of K170 is directly above the Y167 ring and the CE−NZ bond is pointing toward the ring. In the MBP/maltose structure the NZ atom is further away and is not directly above the ring. The CE−NZ bond is parallel to the ring plane and pointing toward the carboxylate oxygens of D180. The distance between the NZ of K170 and the carboxylate oxygen of D180 increases from 2.6 to 3.7 Å in going from the MBP/maltose to the MBP structures (Figure 1). This suggests that the higher magnitude of $\Delta\Delta G°$ in the MBP/maltose is unlikely to result from a stronger cation−π interaction in this structure but instead reflects the loss of the K170−D180 salt bridge in the K170M mutant. Finally, in the case of LIVBP, K248 is hydrogen bonded to the main chain oxygen of P249. Loss of this hydrogen bond in the K248M mutant will contribute to the observed destabilization. The cationic residues mutated in this work can potentially be involved in long-range electrostatic interactions with other charged residues in the protein. A very approximate estimate of this can be obtained by using Coulomb's law with a dielectric constant of 80 as described previously (*44*). In all cases, the total estimated free energy of interaction of the cation with all other charged residues in the protein was in the range of −2 to −3 kcal/mol (data not shown). Removal of these favorable long-range electrostatic interactions will therefore also contribute to any observed destabilization in the mutant proteins. As stated above, the magnitude of the observed $\Delta\Delta G°$ is therefore likely to be an overestimate of cation−π interaction energy.

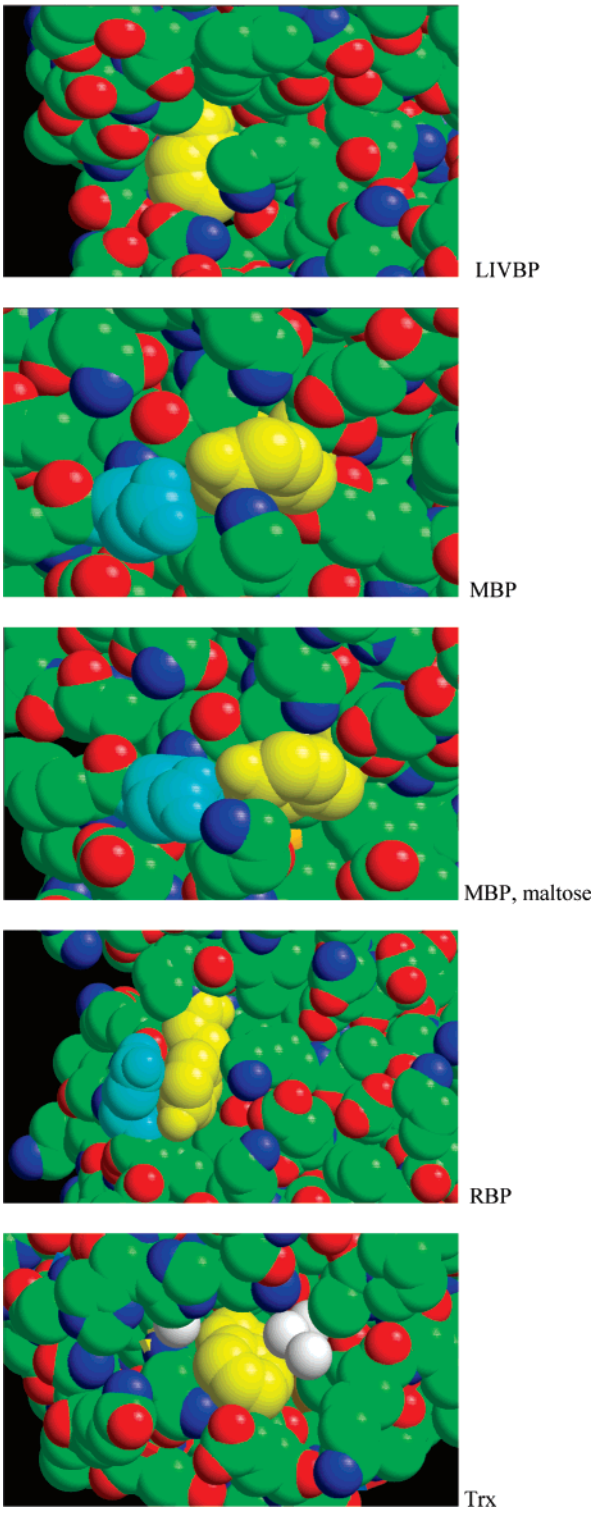

FIGURE 5: Location of aromatic residues that are involved in cation−π interactions and selected for mutation in the structures of WT LIVBP, MBP, MBP/maltose, RBP, and Trx. The aromatic residues is colored yellow, and surrounding residues that are involved in hydrogen bonding with the side chain of the aromatic residue are colored cyan. Water molecules are shown in white. The figure was generated using the program RasTop (*45*). For the remaining residues carbon atoms are in green, oxygen in red, and nitrogen in blue.

CONCLUSIONS

Our results therefore suggest that cation−π interactions are at best weakly stabilizing and may even be destabilizing in some cases at room temperature. However, the stabilizing effect appears to increase at higher temperatures, though this effect may also be due to an increase in the strength of other electrostatic interactions involving the cationic residue at elevated temperature. In the present study, all cation−π pairs studied involved interaction of Lys with either Phe or Tyr or Trp. No pairs involving Arg or Trp could be studied, because, in all four proteins, the cationic residue in such pairs was involved in extensive hydrogen-bonded interactions with other residues. It would be useful to characterize cation−π interactions involving these residues in other proteins to confirm the results of the present study.

ACKNOWLEDGMENT

We thank Dr. S. Mowbray and Dr. L. Luck for expression plamids for WT RBP and LIVBP, respectively. The *E. coli* strain Mri7 was obtained from the *E. coli* Genetic Stock Center, Yale University.

REFERENCES

1. Waters, M. L. (2004) Aromatic interactions in peptides: impact on structure and function, *Biopolymers 76*, 435−445.
2. Burley, S. K., and Petsko, G. A. (1986) Amino-aromatic interactions in proteins, *FEBS Lett. 203*, 139−143.
3. Dougherty, D. A., and Stauffer, D. A. (1990) Acetylcholine binding by a synthetic receptor: implications for biological recognition, *Science 250*, 1558−1560.
4. Beene, D. L., Brandt, G. S., Zhong, W., Zacharias, N. M., Lester, H. A., and Dougherty, D. A. (2002) Cation-pi interactions in ligand recognition by serotonergic (5-HT3A) and nicotinic acetylcholine receptors: the anomalous binding properties of nicotine, *Biochemistry 41*, 10262−10269.
5. Ting, A. Y., Shin, I., Lucero, C., and Schultz, P. G. (1998) Energetic analysis of an engineered cation-pi interaction in staphylococcal nuclease, *J. Am. Chem. Soc. 120*, 7135−7136.
6. Zhong, W., Gallivan, J. P., Zhang, Y., Li, L., Lester, H. A., and Dougherty, D. A. (1998) From ab initio quantum mechanics to molecular neurobiology: a cation-pi binding site in the nicotinic receptor, *Proc. Natl. Acad. Sci. U.S.A. 95*, 12088−12093.
7. Gallivan, J. P., and Dougherty, D. A. (1999) Cation-pi interactions in structural biology, *Proc. Natl. Acad. Sci. U.S.A. 96*, 9459−9464.
8. Wintjens, R., Lievin, J., Rooman, M., and Buisine, E. (2000) Contribution of cation-pi interactions to the stability of protein-DNA complexes, *J. Mol. Biol. 302*, 395−410.
9. Kumpf, R. A., and Dougherty, D. A. (1993) A mechanism for ion selectivity in potassium channels: computational studies of cation-pi interactions, *Science 261*, 1708−1710.
10. Gruber, K., Zhou, B., Houk, K. N., Lerner, R. A., Shevlin, C. G., and Wilson, I. A. (1999) Structural basis for antibody catalysis of a disfavored ring closure reaction, *Biochemistry 38*, 7062−7074.
11. Chakravarty, S., and Varadarajan, R. (2002) Elucidation of factors responsible for enhanced thermal stability of proteins: a structural genomics based study, *Biochemistry 41*, 8152−8161.
12. Olson, C. A., Shi, Z., and Kallenbach, N. R. (2001) Polar interactions with aromatic side chains in alpha-helical peptides: Ch···O H-bonding and cation-pi interactions, *J. Am. Chem. Soc. 123*, 6451−6452.
13. Shi, Z., Olson, C. A., and Kallenbach, N. R. (2002) Cation-pi interaction in model alpha-helical peptides, *J. Am. Chem. Soc. 124*, 3284−3291.
14. Andrew, C. D., Bhattacharjee, S., Kokkoni, N., Hirst, J. D., Jones, G. R., and Doig, A. J. (2002) Stabilizing interactions between aromatic and basic side chains in alpha-helical peptides and proteins. Tyrosine effects on helix circular dichroism, *J. Am. Chem. Soc. 124*, 12706−12714.
15. Tatko, C. D., and Waters, M. L. (2003) The geometry and efficacy of cation-pi interactions in a diagonal position of a designed beta-hairpin, *Protein Sci. 12*, 2443−2452.

16. Ho, S. N., Hunt, H. D., Horton, R. M., Pullen, J. K., and Pease, L. R. (1989) Site-directed mutagenesis by overlap extension using the polymerase chain reaction, *Gene 77*, 51−59.
17. Ames, G. F., Prody, C., and Kustu, S. (1984) Simple, rapid, and quantitative release of periplasmic proteins by chloroform, *J. Bacteriol. 160*, 1181−1183.
18. Beena, K., Udgaonkar, J. B., and Varadarajan, R. (2004) Effect of signal peptide on the stability and folding kinetics of maltose binding protein, *Biochemistry 43*, 3608−3619.
19. Prajapati, R. S., Lingaraju, G. M., Bacchawat, K., Surolia, A., and Varadarajan, R. (2003) Thermodynamic effects of replacements of Pro residues in helix interiors of maltose-binding protein, *Proteins 53*, 863−871.
20. Ganesh, C., Shah, A. N., Swaminathan, C. P., Surolia, A., and Varadarajan, R. (1997) Thermodynamic characterization of the reversible, two-state unfolding of maltose binding protein, a large two-domain protein, *Biochemistry 36*, 5020−5028.
21. Lopilato, J. E., Garwin, J. L., Emr, S. D., Silhavy, T. J., and Beckwith, J. R. (1984) D-ribose metabolism in *Escherichia coli* K-12: genetics, regulation, and transport, *J. Bacteriol. 158*, 665−673.
22. Ghoshal, A. K., Swaminathan, C. P., Thomas, C. J., Surolia, A., and Varadarajan, R. (1999) Thermodynamic and kinetic analysis of the *Escherichia coli* thioredoxin-C′ fragment complementation system, *Biochem. J. 339* (Part 3), 721−727.
23. Holmgren, A., and Reichard, P. (1967) Thioredoxin 2: cleavage with cyanogen bromide, *Eur. J. Biochem. 2*, 187−196.
24. Pace, C. N., Vajdos, F., Fee, L., Grimsley, G., and Gray, T. (1995) How to measure and predict the molar absorption coefficient of a protein, *Protein Sci. 4*, 2411−2423.
25. Chakrabarti, A., Srivastava, S., Swaminathan, C. P., Surolia, A., and Varadarajan, R. (1999) Thermodynamics of replacing an alpha-helical Pro residue in the P40S mutant of *Escherichia coli* thioredoxin, *Protein Sci. 8*, 2455−2459.
26. Lee, H., Chi, S. W., Kang, M., Baek, K., and Kim, H. (1996) Stability and folding of precursor and mature tryptophan-substituted ribose binding protein of *Escherichia coli*, *Arch. Biochem. Biophys. 328*, 78−84.
27. Schellman, J. A. (1987) The thermodynamic stability of proteins, *Annu. Rev. Biophys. Biophys. Chem. 16*, 115−137.
28. Sheshadri, S., Lingaraju, G. M., and Varadarajan, R. (1999) Denaturant mediated unfolding of both native and molten globule states of maltose binding protein are accompanied by large deltaC_p's, *Protein Sci. 8*, 1689−1695.
29. Greene, R. F., Jr., and Pace, C. N. (1974) Urea and guanidine hydrochloride denaturation of ribonuclease, lysozyme, alpha-chymotrypsin, and beta-lactoglobulin, *J. Biol. Chem. 249*, 5388−5393.
30. Ma, J. C., and Dougherty, D. A. (1997) The cation−pi interaction, *Chem. Rev. 97*, 1303−1324.
31. Tsou, L. K., Tatko, C. D., and Waters, M. L. (2002) Simple cation-pi interaction between a phenyl ring and a protonated amine stabilizes an alpha-helix in water, *J. Am. Chem. Soc. 124*, 14917−14921.
32. Tatko, C. D., and Waters, M. L. (2004) Investigation of the nature of the methionine-pi interaction in beta-hairpin peptide model systems, *Protein Sci. 13*, 2515−2522.
33. Stapley, B. J., Rohl, C. A., and Doig, A. J. (1995) Addition of side chain interactions to modified Lifson-Roig helix-coil theory: application to energetics of phenylalanine-methionine interactions, *Protein Sci. 4*, 2383−2391.
34. Wei, Y., Horng, J. C., Vendel, A. C., Raleigh, D. P., and Lumb, K. J. (2003) Contribution to stability and folding of a buried polar residue at the CARM1 methylation site of the KIX domain of CBP, *Biochemistry 42*, 7044−7049.
35. Ponder, J. W., and Richards, F. M. (1987) Tertiary templates for proteins. Use of packing criteria in the enumeration of allowed sequences for different structural classes, *J. Mol. Biol. 193*, 775−791.
36. Biot, C., Buisine, E., Kwasigroch, J. M., Wintjens, R., and Rooman, M. (2002) Probing the energetic and structural role of amino acid/nucleobase cation-pi interactions in protein-ligand complexes, *J. Biol. Chem. 277*, 40816−40822.
37. Richards, F. M. (1977) Areas, volumes, packing and protein structure, *Annu. Rev. Biophys. Bioeng. 6*, 151−176.
38. Pal, D., and Chakrabarti, P. (2001) Non-hydrogen bond interactions involving the methionine sulfur atom, *J. Biomol. Struct. Dyn. 19*, 115−128.
39. Zauhar, R. J., Colbert, C. L., Morgan, R. S., and Welsh, W. J. (2000) Evidence for a strong sulfur-aromatic interaction derived from crystallographic data, *Biopolymers 53*, 233−248.
40. Ratnaparkhi, G. S., and Varadarajan, R. (2000) Thermodynamic and structural studies of cavity formation in proteins suggest that loss of packing interactions rather than the hydrophobic effect dominates the observed energetics, *Biochemistry 39*, 12365−12374.
41. Thomson, J., Ratnaparkhi, G. S., Varadarajan, R., Sturtevant, J. M., and Richards, F. M. (1994) Thermodynamic and structural consequences of changing a sulfur atom to a methylene group in the M13Nle mutation in ribonuclease-S, *Biochemistry 33*, 8587−8593.
42. Elcock, A. H., and McCammon, J. A. (1997) Continuum solvation model for studying protein hydration thermodynamics at high temperatures, *J. Phys. Chem. B 101*, 9624−9634.
43. Dougherty, D. A. (1996) Cation-pi interactions in chemistry and biology: a new view of benzene, Phe, Tyr, and Trp, *Science 271*, 163−168.
44. Pace, C. N., Alston, R. W., and Shaw, K. L. (2000) Charge-charge interactions influence the denatured state ensemble and contribute to protein stability, *Protein Sci. 9*, 1395−1398.
45. Valadone, P., Sayle, R., Mueller, A., and Bernstein, H. (2000) RasTop (version 1.3) (http://www.geneinfinity.org/rastop/).

BI061275F